

DOI: 10.1002/adma.200601098

Nanoscale Domain Control in Multiferroic BiFeO₃ Thin Films**

By Ying-Hao Chu,* Qian Zhan, Lane W. Martin, Maria P. Cruz, Pei-Ling Yang, Gary W. Pabst, Florin Zavaliche, Seung-Yeul Yang, Jing-Xian Zhang, Long-Qing Chen, Darrell G. Schlom, I.-Nan Lin, Tai-Bor Wu, and Ramamoorthy Ramesh

With an ever-expanding demand for data storage, transducers, and microelectromechanical (MEMS) systems applications, materials with superior ferroelectric and piezoelectric responses are of great interest. The lead zirconate titanate (PZT) family of materials has served as the cornerstone for such applications up until now. A critical drawback of this material, however, is the presence of lead and the recent concerns about the toxicity of lead-containing devices. Recently, the lead-free ferroelectric BiFeO₃ (BFO) has attracted a great deal of attention because of its superior thin-film ferroelectric properties,^[1,2] which are comparable to those of the tetragonal, Ti-rich PZT system; therefore, BFO provides an alternate choice as a “green” ferro/piezoelectric material. Another advantage of BFO is its high ferroelectric Curie temperature ($T_c = 850\text{ °C}$ in single crystals),^[3,4] which enables it to be used reliably at high temperatures. The ferroelectric domain structure of epitaxial BFO films are typically discussed in the context of the crystallographic model of Kubel and Schmid,^[5] however, by suppressing other structural variants in BFO, we

can obtain periodic domain structures that may open additional application opportunities for this material.

Ferroelectrics with periodic domain structures are of great interest for applications in photonic devices^[6] and nanolithography.^[7] Such a periodic polarization could be obtained by applying an external electric field while utilizing lithographically defined electrodes or by a direct writing process.^[8,9] To obtain sub-micrometer feature sizes, however, domain engineering using a scanning force microscope with an appropriate bias voltage must be used to fabricate the patterned domain structures.^[10] Unfortunately, this method works only on small areas and is limited by its slow scanning rate. Theoretical models predict the feasibility of controlling the domain architecture in thin films through suitable control over the heteroepitaxial constraints.^[11] In the case of BFO thin films, we have found that such a control is indeed possible, mainly through control over the growth of the underlying SrRuO₃ electrode. Using this approach, we demonstrate the growth of highly ordered 1D ferroelectric domains in 120 nm thick BFO films.

On the (001)_C perovskite surface there are eight possible ferroelectric polarization directions corresponding to four structural variants of the rhombohedral ferroelectric thin film. (For simplicity, the *c* and *o* subscripts refer to the pseudocubic structures for BFO and orthorhombic structures of SrRuO₃ (SRO) and DyScO₃(110)_O (DSO), respectively.) Domain patterns can develop with either {100}_C or {101}_C boundaries for (001)_C-oriented rhombohedral films.^[12] In both cases, the individual domains in the patterns are energetically degenerate and thus equal-width stripe patterns are theoretically predicted. When the spontaneous polarization is included in the analysis, the {100}_C boundary patterns have no normal component of the net polarization, whereas the {101}_C boundary patterns correspond to the fully poled state. The formation of domain patterns leads to the release of elastic energy at the expense of increased interfacial energy associated with the domain boundaries. Therefore, four possible polarization variants still exist when one examines large areas of the sample. If control over the ferroelectric domain structure is desired, one has to recourse to other approaches. In our work, we have used the constraints imposed by heteroepitaxy as well as film-growth mechanisms, shown in Figure 1a, to create long-range order in the domain structure of BFO. First, we use the fact that on the (110)_O surface the DSO lattice is extremely closely matched to that of SRO.^[13] Further, the small structural anisotropy in DSO is used to pin the structure of the SRO layer

[*] Dr. Y.-H. Chu, Dr. Q. Zhan, L. W. Martin, Dr. M. P. Cruz, P.-L. Yang, G. W. Pabst, Dr. F. Zavaliche, Dr. S.-Y. Yang, Prof. R. Ramesh

Department of Materials Science and Engineering &
Department of Physics, University of California
Berkeley, CA 94720 (USA)
E-mail: yhchu@berkeley.edu

Dr. M. P. Cruz
Centro de Ciencias de la Materia Condensada (CCMC)-UNAM
Km. 107 Carretera Tijuana-Ensenada, 22800 Ensenada, B.C.
(Mexico)

J.-X. Zhang, Prof. L.-Q. Chen, Prof. D. G. Schlom
Department of Materials Science and Engineering
Pennsylvania State University
University Park, PA 16802 (USA)

Prof. I.-N. Lin
Department of Physics, Tamkang University
Tamsui, Taiwan 251 (Taiwan)

Prof. T.-B. Wu
Department of Materials Science and Engineering
National Tsing-Hua University
Hsinchu, Taiwan 30013 (Taiwan)

[**] The authors acknowledge support of the National Center for Electron Microscopy, Lawrence Berkeley Lab, which is supported by the U.S. Department of Energy under Contract # DE-AC02-05CH11231. This work is supported by an Office of Naval Research ONR grant no. N00014-06-1-0008 and an ONR-MURI grant no. E-21-6RU-G4. Partial support from a LBL LDRD and a MARCO program, National Science Foundation NSF DMR0122638, NSF DMR-0507146, and a Guggenheim Fellowship is also gratefully acknowledged.

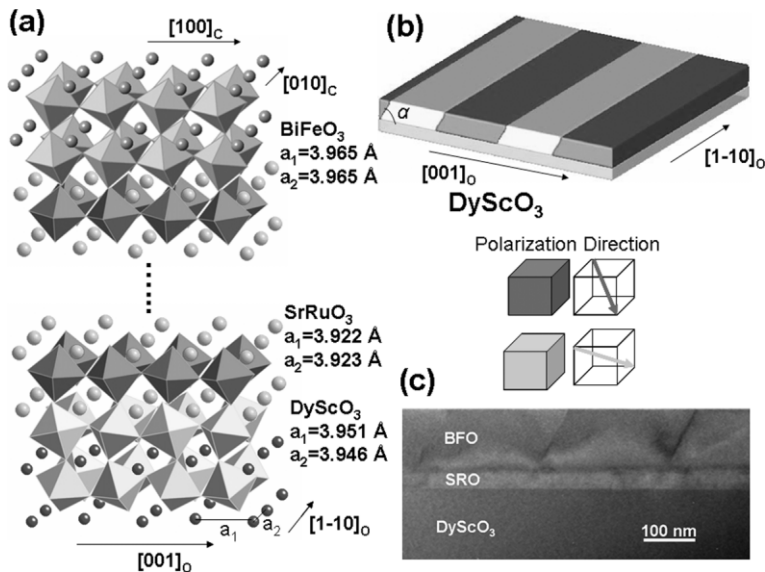


Figure 1. a) Schematic of the BFO/SRO/DSO heterostructure and b) domain structure of BFO film obtained from phase-field simulations. c) The cross-sectional morphology of the films with periodical domain structure.

such that a single-domain variant of the SRO is formed under appropriate growth conditions.

The ferroelectric domain structure of an epitaxial BFO film has been modeled using the phase-field method,^[14] in which the spatial distribution of the polarization field and its evolution is described by the time-dependent Ginzburg–Landau (TDGL) equations.^[15] The domain-wall energy, electrostatic energy, and elastic energy contributions to the total energy are incorporated. A short-circuit electrostatic boundary condition is assumed on both the top surface and the film/electrode interface. The in-plane (IP) lattice parameters are constrained by the underlying (110)_O DyScO₃ substrate with a strain $\epsilon_{11}^E = -0.0035$, $\epsilon_{22}^E = -0.0048$, and $\epsilon_{12}^E = 0$. To predict the domain structure without assuming, a priori, the domain-wall orientations, we started with a paraelectric state plus small random perturbations and annealed the system at room temperature. The domain structure of the film obtained from such a simulation is shown in Figure 1b. It consists of two polarization variants of the rhombohedral phase with downward net polarization. From mechanical compatibility arguments between two variants of a rhombohedral crystal in a 3D bulk system, the domain wall should be parallel to the $\{101\}_C$ plane which is approximately 45° from the film/substrate interface.^[12] How-

ever, our phase-field simulations demonstrate that the domain-wall orientation is a result of the competition between the domain-wall energy and elastic strain energy associated with the domain structure, which leads to a domain-wall surface angle α . The electrostatic energy has no effect on the angle α , since the charge-compatibility condition is fulfilled for any α . (The domain wall is parallel to the $\langle 100 \rangle_C$ direction.) Our phase field calculations show that this angle can change as a function of the domain-wall energy, the film thickness, and the resultant accommodation of misfit in the film; the details of these calculations are the focus of a separate paper.^[16]

The structural domains in SRO^[17] and the resulting BFO domain configuration depends strongly on the substrate vicinal angle and the growth mechanisms. As the SRO growth rate is progressively increased, it is commonly observed that the growth mode changes from step flow to step bunching and finally to island formation.^[18] Based on these observations, careful growth-rate-controlled experiments were performed to enable the observation of these three growth mechanisms in

the SRO layer. The morphology of the SRO films grown by the step-bunching mechanism is shown in Figure 2a. Step bunching can be identified through the formation of unit-cell-high bunched steps, shown by arrows. The presence of circular multiterraces associated with each nucleus suggests that secondary nucleation is taking place on the surface of the bunched steps, which subsequently leads to a multidomain structure in the SRO layer (as shown in Fig. 3). BFO films

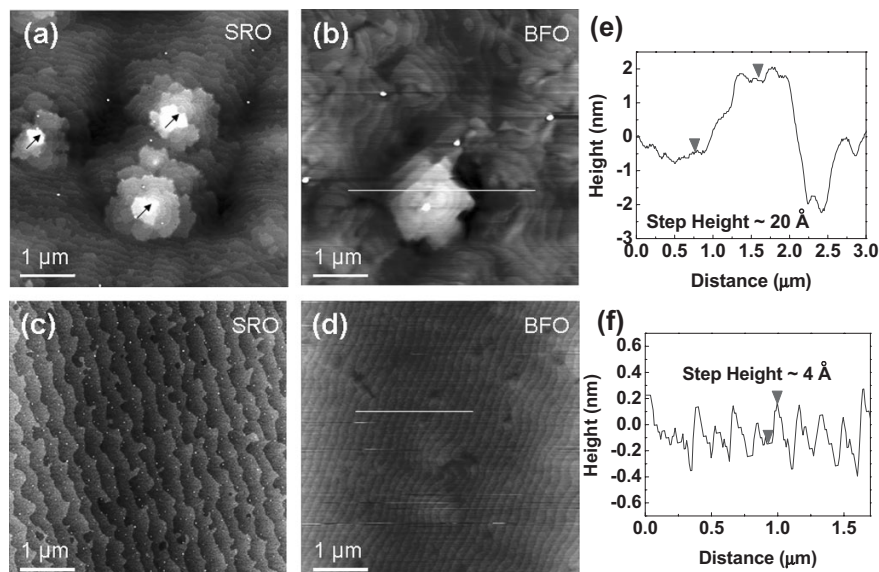


Figure 2. Atomic force microscopy (AFM) images of SRO films grown by a) a step-bunching mechanism and c) a step-flow mechanism. AFM images of BFO films sequentially grown on SRO films by b) step bunching and d) step flow. e,f) Section analysis along the line drawn in (b) and (d), respectively.

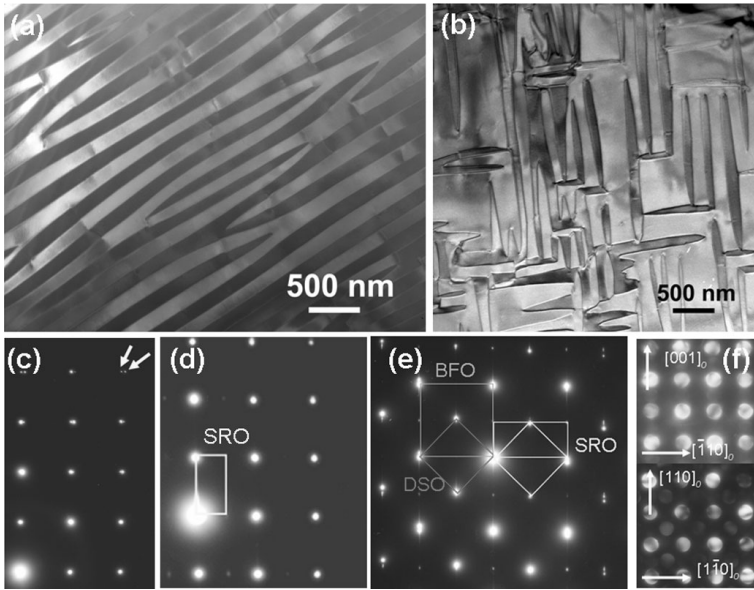


Figure 3. Typical plan-view bright-field image of BFO films with a) periodic domain structure and b) multidomain structure. Corresponding c) plane-view and d) cross-sectional electron diffraction patterns (EDPs) of BFO films with periodical domain. Corresponding e) cross-sectional EDP and f) microdiffraction patterns of BFO films with multidomain structure.

mation is shown in Figure 4b. When the growth rate is slowed down, however, the SRO film shows a periodic step pattern with well-aligned steps, indicating that step flow growth has occurred (Fig. 2c). BFO films grown on these SRO surfaces likewise mimic the topography of the underlying SRO films (Fig. 2d). Due to the coherent growth, the film surface shows large terraces, roughly 200 nm in diameter, that are atomically flat and separated by small steps varying between half and one unit cell in height (Fig. 2f); the corresponding ferroelectric domain information is shown in Figure 4d. The film surface, therefore, is extremely smooth with a root-mean-square (rms) roughness of 2.7 Å over a 5 μm × 5 μm scan area.

The crystallographic orientation relationships, as well as the correlation between the domains in SRO and BFO, were examined using transmission electron microscopy (TEM). The 1D periodic domain structure was investigated looking down the [001]_C zone axis. Figure 3a shows a typical plan-view bright-field image of the film and corresponding electron diffraction pattern (EDP) (Fig. 3c) along the [110]_O zone axis of DSO. A striplike parallel domain structure aligned along the [010]_C direction was observed. Each domain has an average

width of approximately 200 nm. The IP lattice parameters were calculated as 3.956 and 3.944 Å in a magnified quadrant of the EDP (Fig. 3c). The smaller IP lattice parameter perpendicular to the strip domain corresponds to the smaller lat-

width of approximately 200 nm. The IP lattice parameters were calculated as 3.956 and 3.944 Å in a magnified quadrant of the EDP (Fig. 3c). The smaller IP lattice parameter perpendicular to the strip domain corresponds to the smaller lat-

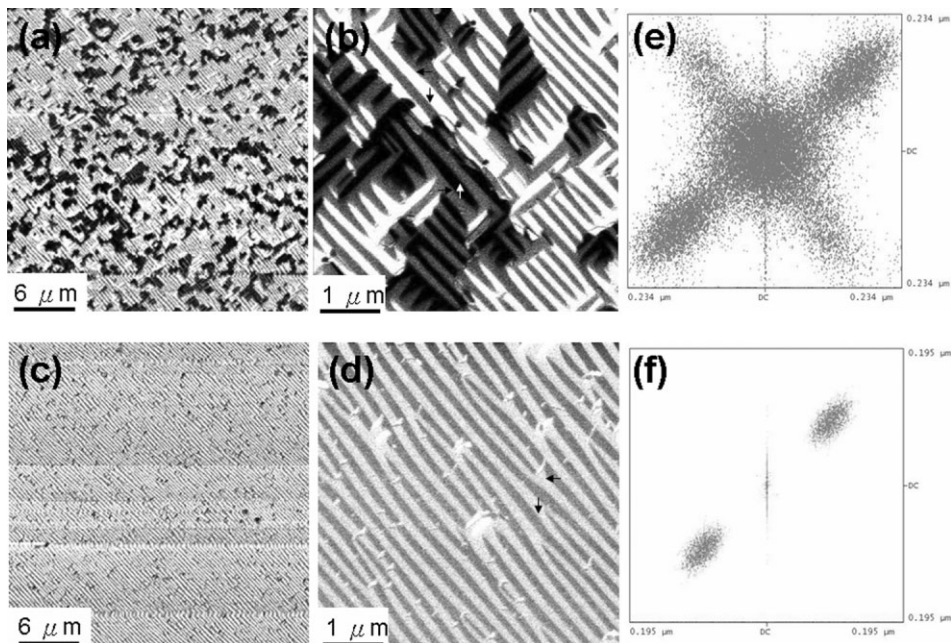


Figure 4. a) Large-area (30 μm × 30 μm) in-plane piezoforce microscopy (IP-PFM) image of BFO films with multidomain structure and b) the corresponding IP-PFM images of Figure 2c; c) large-area (30 μm × 30 μm) IP-PFM image of BFO films with periodical domain structure and d) the corresponding IP-PFM images of Figure 2d. The arrows represent the directions of IP polarization components. e, f) ODPs obtained from the corresponding PFM images (a) and (c), respectively.

tice parameter on SRO, revealing the role of heteroepitaxy. The spot splitting in the selected-area electron diffraction (SAD) pattern reveals a misorientation of approximately 1.1° between two adjacent domains. For a rhombohedrally distorted BFO structure, the spontaneous distortion angle, α , is 89.4° ,^[5] which means the misorientation angle is 1.2° for a 71° rotation of the polarization direction between adjacent stripe domains; this is consistent with the misorientation angle measured from the SAD patterns. The cross-sectional morphology of the films confirms the domain width and the direction of the domain boundary, which is in agreement with theoretical calculations (Fig. 1c). In contrast, the BFO films grown on SRO layers with multiple structural domains show a 2D hatch of ferroelectric domains. Figure 3b shows the plane-view bright-field image for one such sample, which confirms the multidomain structure imaged in piezoforce microscopy images. The domain boundaries show traces along the $[100]_C$ and $[010]_C$ crystallographic directions.

The cross-sectional EDP of the 1D periodic structure is shown in Figure 3d. It is worth noting that SRO exhibits monodomain structure in this film since there are no extra diffraction spots besides the ones recorded from the $[\bar{1}10]_O$ zone axis. In contrast, the samples in which the SRO was grown via the step-bunching mechanism showed two sets of SRO structural domains, as identified by the EDPs in Figure 3e. Further confirmation is obtained from electron microdiffraction patterns obtained from each of these structural domains and shown in Figure 3f. These microdiffraction patterns can be uniquely indexed to be the $[001]_O$ and $[1\bar{1}0]_O$ zone axes of SRO.

Piezoforce microscopy (PFM) images reflect the dramatic differences in structure shown in Figures 2 and 3. IP-PFM images of the BFO films grown on the multidomain SRO films (Fig. 4b), taken with the cantilever along the $\langle 110 \rangle_C$ direction, show two orthogonal sets of domains. The three contrasts seen in the IP-PFM images acquired along two orthogonal $\langle 110 \rangle_C$ directions, together with the uniform out-of-plane (OP) PFM contrast, tell us that BFO's domain structure is characterized by four polarization variants.^[19] The large-area scan shown in Figure 4a proves that this periodic array of domains is a stable configuration over large length scales. In contrast, for BFO films grown on SRO films exhibiting the step-flow growth mode, the IP-PFM scans, taken along any $\langle 110 \rangle_C$ direction, show only two contrasts over large areas (Fig. 4c) in a stripe configuration (Fig. 4d). PFM images obtained from various parts of the same sample reveal images with the same stripe orientation, further suggesting that this pattern likely extends over the whole sample and corresponds to two downward directed polarization variants that are 71° apart. We emphasize here that the substrate terrace structure, which typically lies along the $[001]_O$ direction, is different

from the direction of the stripe domains. This result is in agreement with the stable configuration predicted for a $(001)_C$ oriented rhombohedral ferroelectric film. Optical diffraction patterns (ODPs) obtained from these PFM images, Figure 4e and f, yield an average stripe-domain width of approximately 200 nm. They also reflect the symmetry of the domains in the two types of films; in the stripe-dominated sample, only one set of diffraction spots is observed, while the film with two sets of stripes shows two orthogonal sets of diffraction spots. The ODPs also reveal sharp diffraction maxima, suggesting a strong degree of coherence normal to the stripes.

Such 1D periodic structure reflects on the high quality of these BFO films. The macroscopic electrical polarization-field (P - E) hysteresis loops with different measuring frequency of the BFO films are shown in Figure 5a, showing sharp, square loops and yield a $2P_r$ (P_r : remanent polarization) value of $120 \mu\text{C cm}^{-2}$. Sharp ferroelectric loops can be obtained even at a low frequency of 200 Hz and leakage measurements indicate low leakage levels ($<10^{-7}$ A) at 10 V (Fig. 5b). It is also interesting to explore the reversibility of such a 1D stripe-domain structure when the domain structure is switched with electric fields. Preliminary work in this direction, shown in Figure 5c and d, suggests that this may indeed be possible. Application of alternate +6 V/-6 V DC voltages switches the IP and OP components of the polarization. The OP component reverses contrast from bright to dark and therefore does not reveal critical information. The IP images, on the other hand, clearly show that the stripe nature is maintained, although the stripe spacing appears to be doubled.

In conclusion, we have demonstrated self-oriented ferroelectric domains in BFO films with 1D periodic structure on the order of 200 nm. By careful control of the growth mecha-

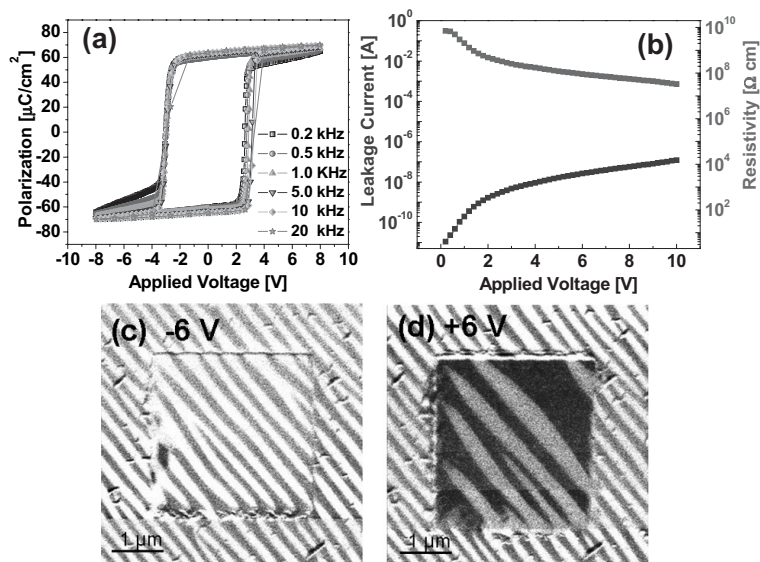


Figure 5. a) The macroscopic electrical P - E hysteresis loops with different measuring frequency, and b) leakage current and resistivity versus applied voltage of the BFO films. IP-PFM images of alternate c) -6 V and d) $+6$ V DC voltages.

nism for the SRO layer, the IP lattice parameters of SRO films are pinned by DSO substrate to create the 1D periodic domain structure.

Experimental

In order to facilitate high-quality heteroepitaxy, we have used single-crystalline DSO substrates. In addition to providing the appropriate perovskite template, DSO is very closely lattice matched to the orthorhombic structure of SRO (Fig. 1a). Epitaxially grown films of SRO with thicknesses of 40 nm were used as bottom electrodes because of its close lattice match with both BFO and DSO. The crystallinity of the BFO/SRO/DSO films was studied using TEM (CM200 FEG operating at 200 kV and JEOL 3010 operating at 300 kV). The morphology and local piezoelectric properties of these heterostructures were investigated using an atomic force microscope based setup [19], which was performed in a DI Multimode atomic force microscope. Pt top electrodes (32 μm in diameter) were patterned to measure the ferroelectric properties with an RT-6000 ferroelectric testing station.

Received: May 19, 2006

Final version: June 24, 2006

Published online: August 8, 2006

- [1] J. Wang, J. B. Neaton, H. Zheng, V. Nagarajan, S. B. Ogale, B. Liu, D. Viehland, V. Vaithyanathan, D. G. Schlom, U. V. Waghmare, N. A. Spaldin, K. M. Rabe, M. Wuttig, R. Ramesh, *Science* **2003**, 299, 1719.
- [2] S. Y. Yang, F. Zavaliche, L. Mohaddes-Ardabili, V. Vaithyanathan, D. G. Schlom, Y. J. Lee, Y. H. Chu, M. P. Cruz, Q. Zhan, T. Zhao, and R. Ramesh, *Appl. Phys. Lett.* **2005**, 87, 102903.
- [3] Y. N. Venetsev, G. Zhadanov, S. Solov'ev, *Sov. Phys. Crystallogr.* **1960**, 4, 538.
- [4] G. Smolenskii, V. Isupov, A. Agranovskaya, N. Kranik, *Sov. Phys. Solid State* **1961**, 2, 2651.
- [5] F. Kubel, H. Schmid, *Acta Crystallogr. Sect. B* **1990**, 46, 698.
- [6] V. Berger, *Phys. Rev. Lett.* **1998**, 81, 4136.
- [7] S. V. Kalinin, D. A. Bonnell, T. Alvarez, X. Lei, Z. Hu, R. Shao, J. H. Ferris, *Adv. Mater.* **2005**, 17, 795.
- [8] C. Restoin, C. Darraud-Taupiac, J. L. Decossas, J. C. Vareille, *J. Appl. Phys.* **2000**, 88, 6665.
- [9] X. Li, K. Terabe, H. Hatano, K. Kitamura, *Jpn. J. Appl. Phys.* **2005**, 44, L1550.
- [10] X. Liu, K. Terabe, M. Nakamura, S. Takezawa, K. Kitamura, *J. Appl. Phys.* **2005**, 97, 064308.
- [11] Y. L. Li, S. Y. Hu, L. Q. Chen, *J. Appl. Phys.* **2005**, 97, 034112.
- [12] S. K. Streiffer, C. B. Parker, A. E. Romanov, M. J. Lefevre, L. Zhao, J. S. Speck, W. Pompe, C. M. Foster, G. R. Bai, *J. Appl. Phys.* **1998**, 83, 2742.
- [13] J. Schubert, O. Trithaveesak, A. Petraru, C. L. Jia, R. Uecker, P. Reiche, D. G. Schlom, *Appl. Phys. Lett.* **2003**, 82, 3460.
- [14] L. Q. Chen, *Annu. Rev. Mater. Res.* **2002**, 32, 113.
- [15] Y. L. Li, S. Y. Hu, Z. K. Liu, L. Q. Chen, *Appl. Phys. Lett.* **2001**, 78, 3878.
- [16] J. X. Zhang, S. Choudhury, Y. L. Li, Y. H. Chu, F. Zavaliche, Q. X. Jia, D. G. Schlom, R. Ramesh, L. Q. Chen, unpublished.
- [17] R. A. Rao, Q. Gan, C. B. Eom, *Appl. Phys. Lett.* **1997**, 71, 1171.
- [18] W. Hong, H. N. Lee, M. Yoon, H. M. Christen, D. H. Lowndes, Z. Suo, Z. Zhang, *Phys. Rev. Lett.* **2005**, 95, 095501.
- [19] F. Zavaliche, R. R. Das, D. M. Kim, S. Y. Yang, P. Shafer, C. B. Eom, R. Ramesh, *Appl. Phys. Lett.* **2005**, 87, 182912.